


Multifunctional Chitin Nanogels for Simultaneous Drug Delivery, Bioimaging, and Biosensing

Sanoj Rejinold N,[†] Krishna Prasad Chennazhi,[†] Hiroshi Tamura,[‡] Shantikumar V. Nair,[†] and Rangasamy Jayakumar^{*,†}

[†]Amrita Centre for Nanosciences and Molecular Medicine, Amrita Institute of Medical Sciences and Research Centre, Amrita Vishwa Vidyapeetham University, Kochi 682041, India

[‡]Faculty of Chemistry, Materials and Bioengineering, Kansai University, Osaka 564-8680, Japan

 Supporting Information

ABSTRACT: In this work, we developed biodegradable chitin nanogels (CNGs) by controlled regeneration method. For multifunctionalization, we have conjugated CNGs with MPA-capped-CdTe-QDs (QD-CNGs) for the *in vitro* cellular localization studies. In addition, the Bovine Serum Albumin (BSA) was loaded on to QD-CNGs (BSA-QD-CNGs). The CNGs, QD-CNGs, and BSA-QD-CNGs were well-characterized by SEM and AFM, which shows that the nanogels are in the range of <100 nm. These were further characterized by FT-IR and Cyclic Voltametry. The cytocompatibility assay showed that the nanogels are nontoxic to L929, NIH-3T3, KB, MCF-7, PC3, and VERO cells. The cell uptake studies of the QD-CNGs were analyzed, which showed retention of these nanogels inside the cells (L929, PC3, and VERO). In addition, the protein loading efficiency of the nano gels has also been analyzed. Our preliminary studies reveal that these multifunctionalized nanogels could be useful for drug delivery with simultaneous imaging and biosensing.

KEYWORDS: chitin nanogels, multifunctional, cellular localization, drug delivery, imaging, biosensor

INTRODUCTION

“Chitin nano biomaterials” is an upcoming field in the biotechnology field, having lot of applications in drug delivery and tissue engineering.¹ After significant advances in the fabrication of a wide variety of functional nanomaterials, there has been a growing interest in the multifunctionalization into a single nano object.^{2–10} The unique optical properties such as wideband excitation, narrow emission, phenomenal photostability and high quantum yield of Quantum dots (QDs) are making them as a potential candidate for bioimaging and labeling probes.^{1–8} Biopolymers have been widely utilized for the multifunctionalization of various nanoformulations. Their amenability to surface conjugation with QDs helps to combine the imaging modality with therapy.^{10–13} In general, QDs have lower drug loading capacity, which resulted in very nonuniform release kinetics even in response to local environment. Nanogels are hydrogels confined to nanoscopic dimensions with many attractive properties such as size tunability, large surface area useful for multivalent bioconjugation, excellent drug loading capacity, controlled release, and their responsiveness to environmental stimuli. These properties make them very attractive to be an ideal drug delivery system.^{14–17} Natural polymers like chitin are widely used in the biomedical field because of their high biocompatibility and the enriched functionalities being capable of functionalize well with variety of ligands. Chitin is composed of β -1,4 linked units of the amino sugar N-acetyl-glucosamine, and is the main source of production of chitosan.^{18–30}

Although significant benefits have been achieved on the relative areas, to the best of our knowledge, there are no studies that refer to the nano biopolymer-based on chitin for simultaneous sensing, imaging and therapy. Here, we developed a class of chitin nanogels (CNGs) ($R_n < 100$ nm) and their preliminary

multifunctionalization capabilities with QDs and Bovine Serum Albumin (BSA) as model protein. In our study, CNGs have been conjugated with CdTe QDs (3.2–3.8 nm) by *in situ* immobilization in the CNGs network, which should display the properties and functions from each building blocks, as schematically depicted in Figure 1. Chitin is distinct from other commonly available polysaccharides due to its glucosamine groups, and capacity to form polyelectrolyte complexes, making it a very versatile material with extensive application in the biomedical and biotechnological fields.^{31,32} In addition, the rich –OH and –NHCOCH₃ groups of chitin chains should be able to interact with Cd²⁺ ions into the gel network and stabilize the *in situ* formed CdTe QDs embedded in the gel network.^{33–36} The designed chitin-based nanogels and their multifunctionalized formulations can interconnect the pH-sensing, cancer cellular imaging, delivering drugs under the local environmental stimuli hold a great promise for simultaneous diagnosis, therapy, and monitoring on the response to drug treatments.

EXPERIMENTAL SECTION

Materials. α -Chitin with molecular weight of 150 kDa and degree of acetylation –72.4% was purchased from Koyo chemical Co., Ltd., Japan. CaCl₂ and methanol were purchased from Qualigens, India. Cadmium Chloride hemi (Pentahydrate) (CdCl₂, molecular weight 228.36), Tellurium powder, 200 mesh (99.997%) and mercaptopropionic acid, (>99%) were purchased from Sigma Aldrich. Sodium hydroxide pellets (ExcelsaR grade) was purchased from Fischer Scientific. Sodium borohydride was purchased from Qualigens. The cell lines were provided by

Received: June 29, 2011

Accepted: August 24, 2011

Published: August 24, 2011

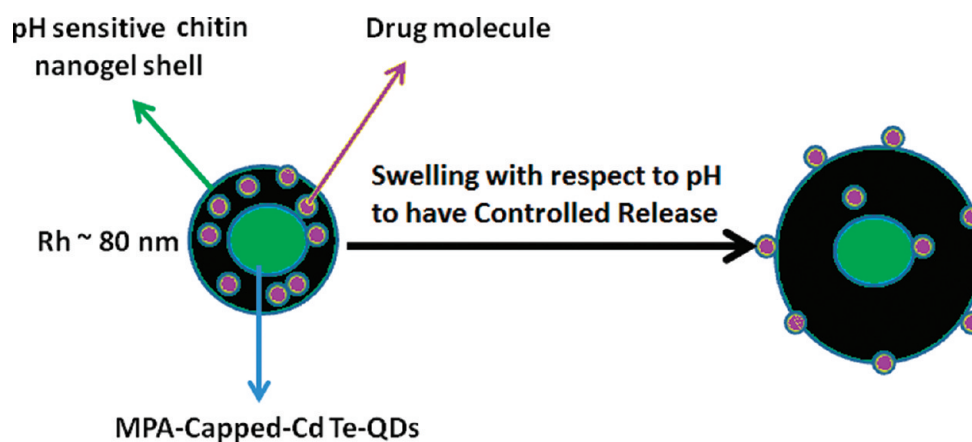


Figure 1. Schematic representation for the concept for designing multifunctional BSA loaded-CdTe QDs-chitin hybrid nanogel (BSA-QD-CNGs) and its potential extending applications in the biomedical field.

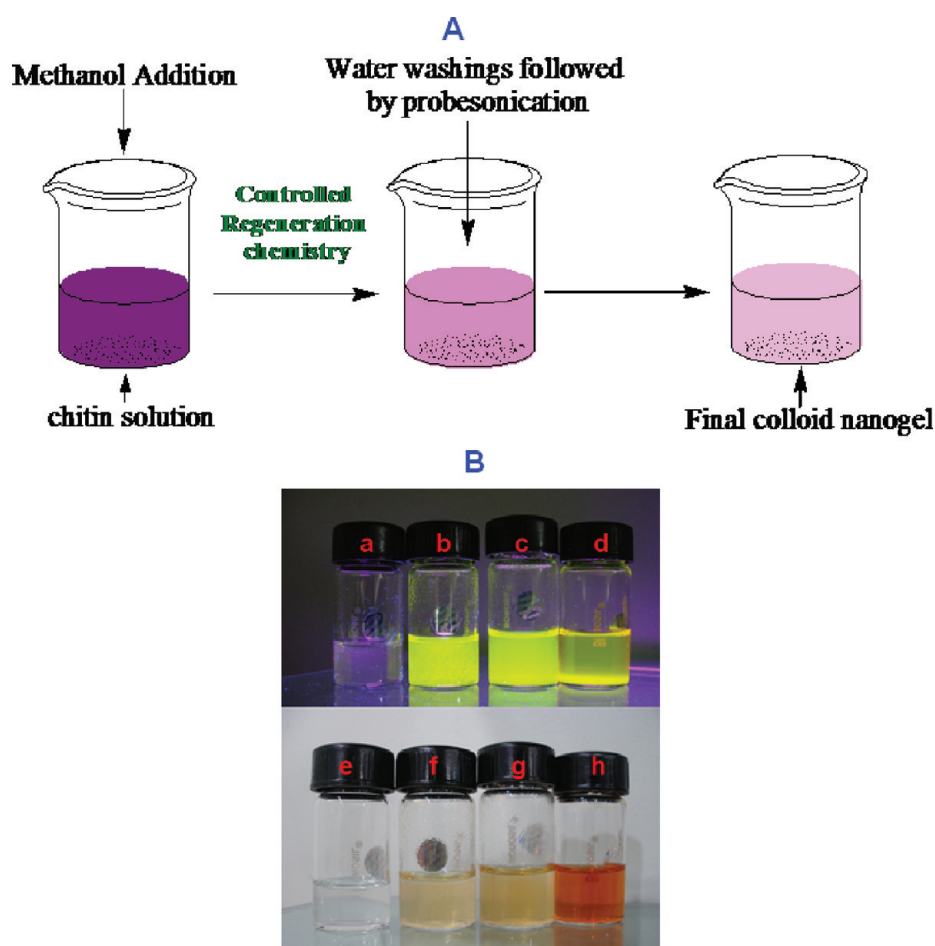


Figure 2. (A) Synthesis route for the chitin nanogels (CNGs) by controlled regeneration chemistry. (B) UV-exposed samples of (a) CNGs, (b) BSA-QD-CNGs, (c) QD-CNGs, and (d) bare QDs; (e–h) same samples under normal light.

National Center for Cell Sciences (NCCS), Pune, India. The chemicals were used without further purification.

Synthesis of Nanogels by Controlled Regeneration Chemistry.

Preparation of Chitin Solution. Chitin solution was prepared according to the reported literature.³⁷ Briefly, chitin was dissolved in saturated CaCl_2 /methanol solvent and stirred vigorously for 48 h at room temperature. After getting a transparent chitin solution, it was filtered to remove the undissolved traces.

Synthesis of Chitin Nanogels (CNGs). The chitin solution (10 mL) (which contains 0.5 mg/mL chitin; 65 g of CaCl_2 in 65 mL of methanol) was stirred for an hour, under controlled stirring at room temperature followed by dropwise addition of methanol (twice the volume of the gel solution) until get a regenerated chitin gels, a clear turbid solution. The above solution then washed several times with water until the whole methanol gets completely removed out from the CNGs. The nanogels

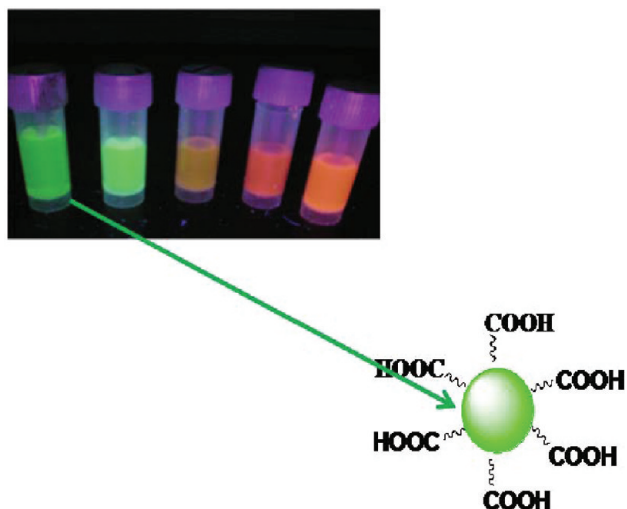
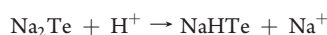
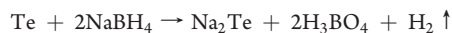


Figure 3. Coating mechanism of the MPA on the CdTe-QDs. Photograph of CdTe QDs of different sizes, luminescence varying from bright green to red under UV lamp (Inset).

should be centrifuged with water followed by higher amplitude (75%) probe sonication for 5 min, and then resuspended in water for further studies. A schematic representation for the synthesis has been shown in Figure 2A.

Synthesis of MPA-Capped-CdTe-QDs. CdTe QDs were prepared by aqueous route slightly modified and optimized from the one described in the literature.³⁸

Preparation of Tellurium Precursor. Tellurium is reduced sodium borohydride (NaBH₄), sodium hydrogen telluride (NaHTe).



0.018 g of Tellurium powder (Te) and 0.45 g of sodium borohydride (NaBH₄) are added into a single-neck RB flask with 10 mL of water in it. The solution is stirred in oxygen-free environment until a clear solution with no sediments of tellurium is obtained and outlet is provided for release of hydrogen gas from the reaction.

Preparation of Cadmium Precursor. 0.078 g of cadmium Chloride hemi (Pentahydrate) (CdCl₂ · Five H₂O) and 125 mL of water (milli-Q) are taken in a 200 mL beaker, and the solution is stirred well with the help of a glass rod until the cadmium is dissolved properly. Then, 235 μL of mercaptopropionic acid (MPA) is added in to the solution, then the pH of the solution is brought to 11.9 according to the literature³⁸ with the help of 1 M NaOH.

Preparation of Cadmium Telluride. Purge the cadmium precursor in nitrogen gas for 15 min and add the tellurium precursor into it before oxidation happens. Then, keep the CdTe precursor at temperature 98 °C with stirring. On the basis of the luminescence observed by the solution under an UV lamp, samples are collected over duration in regular intervals.

CdTe QDs Conjugation with the CNGs (QD-CNGs). The MPA-capped CdTe QDs were incorporated with CNGs via physical adsorption chemistry. The QDs were prepared via a simple aqueous route, so we incorporated the QDs with the nanogels in aqueous conditions only. Briefly, the QDs (500 μL) were mixed with 2 mL CNGs (which contains 5 mg/mL chitin content) at constant stirring for 30 min in the room temperature. The unreacted hydroxyl and/or amine residues are capable of making strong bonds with the Cd²⁺ ions. Even though the incorporation is via physical route, the bonding would be high enough to hold the

QDs with CNGs, which is having strong functionalities such as –NH₂, –OH, and –NHCOCH₃. The weight contents of each component in the QD-CNGs and BSA-QD-CNGs have been tabulated in the Supporting Information, Table 1.

Loading Efficiency of CNGs and QD-CNGs for BSA. For these studies, we have selected BSA as a model protein drug. Prior to the loading of BSA in QD-CNGs, we analyzed the loading efficiency of the control CNGs, by varying the BSA concentration as 5, 10, 20, and 40%. The successful completion of this work allowed us to further move on with BSA loading on QD-CNGs. The BSA can load on QD-CNGs through physical adsorption chemistry. Briefly, the BSA (5 mg/mL) in water was mixed QD-CNGs (50 mg), thereby confirming, most of the BSA proteins would be entrapped inside the nanogels. 10% BSA was encapsulated inside the nanogels.

The percentage of BSA incorporated with nanogels was determined by centrifuging the BSA-loaded nanogels at 8000 rpm for 3 min and supernatant was measured by UV spectrophotometer (UV-1700 Pharma Spec) at 280 nm by dissolving the supernatant containing released BSA in water. The calculated loading efficiency (LE) was ~92% using the following formula.

$$\text{LE (\%)} = \frac{\text{total amount of BSA} - \text{free BSA}}{\text{total amount of BSA}} \times 100\%$$

Lyophilization of the CNGs and BSA-QD-CNGs. The CNGs and BSA-QD-CNGs can be lyophilized by dispersing in milli pore water followed by overnight incubation of the samples at –85 °C, and the frozen samples can then immediately be lyophilized for 48 h to get the powdered samples for the characterization and cell culture studies.

In vitro Quantification of BSA. For *in vitro* quantification of BSA, a standard solution of BSA in PBS was prepared by dissolving 5 mg of BSA in 100 mL of PBS solution. A serial dilution from 0.2 to 2 mL was done and diluted to 25 mL and its absorbance was measured at 280 nm using (UV-1700 Pharma Spec) UV spectrophotometer. The readings were plotted to get a straight line for the quantification of unknown BSA present in the nanogels.

In vitro Protein Release. A known amount of lyophilized CNGs and BSA-QD-CNGs (50 mg in 20 mL milli pore water) was dispersed in 10 mL of phosphate buffers of pH 7.4 and 4.5, respectively, and the solution was divided into 30 eppendorf tubes (500 μL each; 3 sets for pH 4.5 and 3 sets for pH 7.4). The tubes were kept in a thermostable water bath set at 37 °C. Free BSA is completely soluble in water; therefore at predetermined time intervals, the solution was centrifuged at 8000 rpm for 3 min to separate the released BSA (in the supernatant) from the CNGs and QD-CNGs. The BSA, which was released have withdrawn from each eppendorf tubes according to the time intervals to spectrophotometrically measure at 280 nm. The concentration of released BSA was then calculated using standard curve of BSA in PBS. The percentage of BSA released was determined from the following equation

$$\text{release (\%)} = \frac{\text{released BSA from CNGs and QD-CNGs}}{\text{total amount of BSA in CNGs and QD-CNGs}} \times 100\%$$

Cell Lines and Culture Protocols. L929 (mouse fibroblast cell line), NIH-3T3 (mouse embryonic fibroblast cell line), KB (oral cancer cell line), VERO cells (kidney epithelial cell line of the African Green Monkey), MCF-7 (Human Breast cancer cell line) purchased from NCCS Pune, which were maintained in Minimum Essential Medium (MEM) and PC3 (prostate cancer cell lines, NCCS Pune) was maintained in Dulbecco's modified Eagles Medium (DMEM) F12 supplemented with 10% fetal bovine serum (FBS). The cells were incubated in

CO₂ incubator with 5% CO₂. After reaching confluency, the cells were detached from the flask with trypsin-EDTA. The cell suspension was

centrifuged at 3 000 rpm for 3 min and then resuspended in the growth medium for further studies.

Cell Uptake Studies by Fluorescent Microscopy. Acid etched coverslips kept in 24 well plates were loaded with L929, VERO and PC3 cells with a seeding density of 5000 cells per coverslip and incubated for 24 h for the cells to attach well. After the 24 h incubation, the media was removed and the wells were carefully washed with PBS buffer. Then the QD-CNGs of size 80 nm at a concentration of 1 mg/mL (where the concentration of QDs is 3.9 μg) was added along with the media in triplicate to the wells and incubated for 2 and 24 h. Thereafter the media with samples were removed and the coverslips were processed for fluorescent microscopy. The processing involved washing the coverslips with PBS and thereafter fixing the cells in 3.7% para formaldehyde (PFA) followed by a final PBS wash. The coverslips were air-dried and mounted on to glass slides with DPX as the mountant medium. The slides were then viewed under the fluorescent microscope.

Cytotoxicity Studies. For cytotoxicity experiments, L929, NIH-3T3, VERO, MCF7, PC3, and KB cells were seeded on a 96-well plate with a density of 10,000 cells/cm². MTT [3-(4, 5-Dimethylthiazole-2-yl)-2,5-diphenyl tetrazolium] assay, a colorimetric test based on the selective ability of viable cells to reduce the tetrazolium component of MTT in to purple colored formazan crystals was used to evaluate cytotoxicity of the prepared nanogels. Six different concentrations of the nanogels (0.1, 0.2, 0.4, 0.6, 0.8, and 1 mg/mL; where the BSA concentration varied from 0.9 to 8.6 μg and QDs concentration varied from 0.25, 0.50, 1.0, 2.0, and 3.9 μg) were prepared by dilution with the media. After reaching 90% confluency, the cells were washed with PBS buffer and different concentration of the nanogels (100 μL) were added and incubated. Cells in media alone devoid of nanogels acted as negative control and wells treated with triton X-100 as positive control for a period of 24 h. 5 mg of MTT (Sigma) was dissolved in 1 mL of PBS and filter sterilized. 10 μL of the MTT solution was further diluted to 100 μL with 90 μL of serum-free phenol red free medium. The cells were

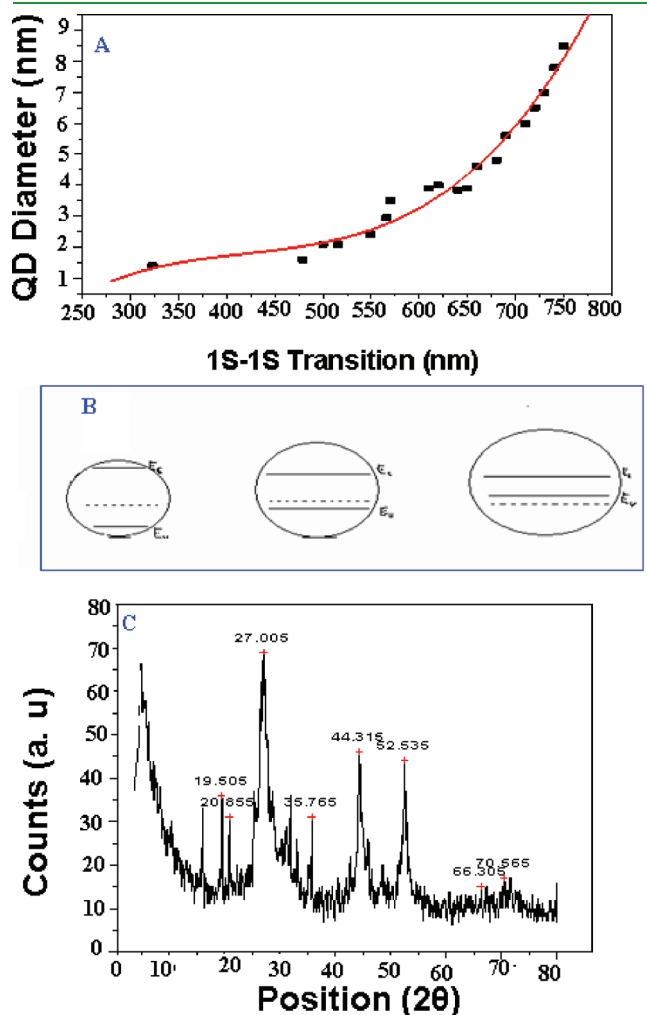


Figure 4. (A) Sizing curve for MPA-capped-CdTe QDs synthesized in water. (B) Schematic diagrams of energy levels of traps (dotted lines) for QD-CNGs with increasing sizes and (C) XRD of MPA-capped CdTe QDs.

Table 1. Showing the Particle Size Parameters for the CNGs with Respect to the Time and Amplitude of Probe Sonication

samples	probing time (min)	probing amplitude %	particle size measured in DLS (nm)
CNGs (a)	1	25	200 ± 2
CNGs (b)	2	45	150 ± 7
CNGs (c)	3	60	100 ± 5
CNGs (d)	5	75	30 ± 15

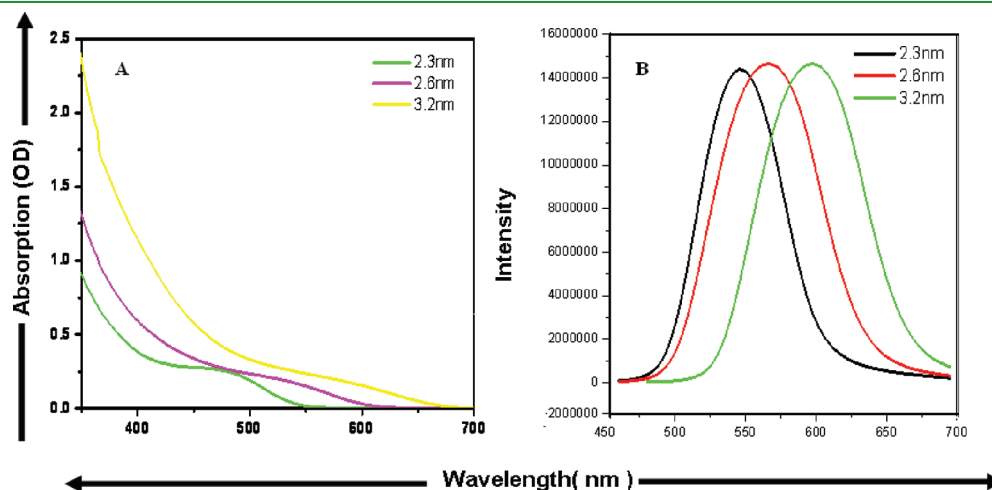


Figure 5. (A) Absorption Spectra and (B) PL spectra of different sized CdTe QDs.

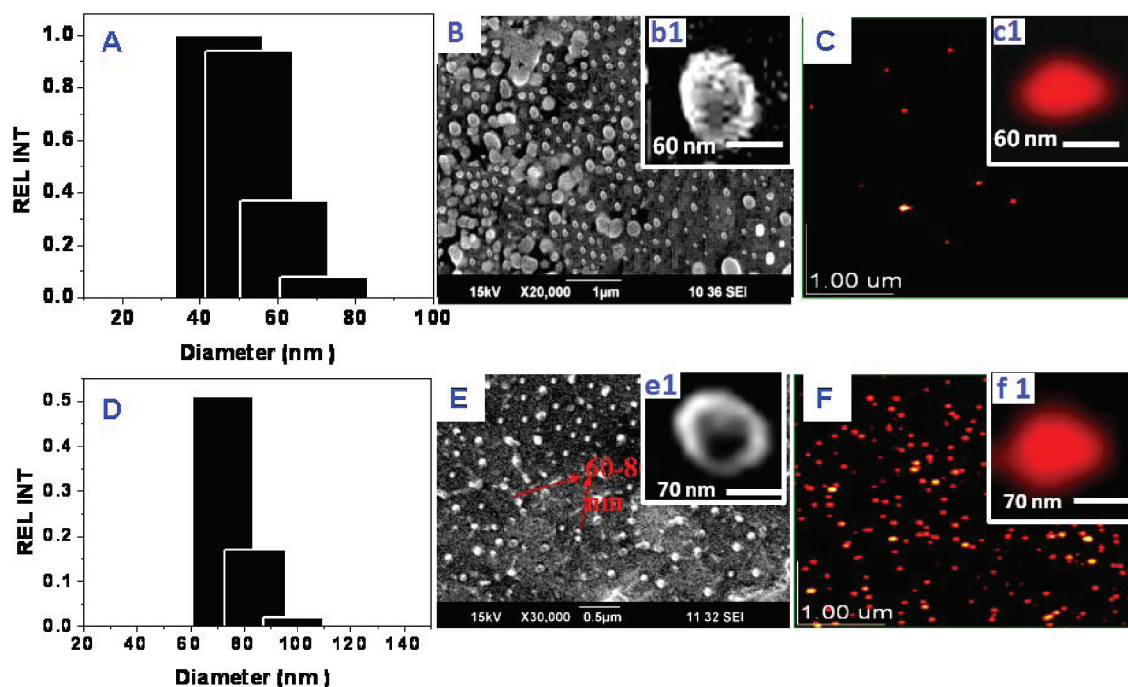


Figure 6. Size distribution of CNGs and BSA-QD-CNGs. (A–C) DLS, SEM, and AFM analysis of CNGs and (D–F) the same for BSA-QD-CNGs. Magnified SEM (b1, e1) and AFM (c1, f1) images for CNGs and BSA-QD-CNGs.

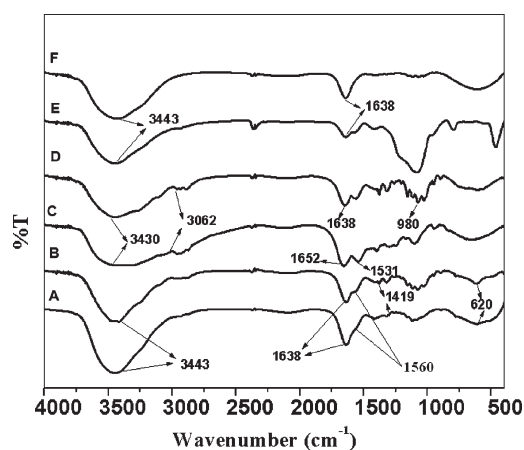


Figure 7. FT-IR of (A) chitin (control), (B) CNGs, (C) BSA (control), (D) BSA-CNGs, (E) MPA-capped CdTe QDs, and (F) BSA-QD-CNGs.

incubated with 100 μL of the above solution for 4 h to form formazan crystals by mitochondrial dehydrogenases. 100 μL of the solubilization solution (10% triton X-100, 0.1N HCl and isopropyl alcohol) was added in each well and incubated at room temperature for 1 h to dissolve the formazan crystals. The optical density of the solution was measured at a wavelength of 570 nm using a Beckmann Coulter Elisa plate reader (BioTek Power Wave XS). Triplicate samples were analyzed for each experiment.

Hemolysis Assay. Blood compatibility was evaluated with hemolysis assay. Ten mL Fresh human blood was treated with 1.5 mL acid citrate dextrose (ACD) and 100 μL of sample of concentration ranging from 0.2 to 2 mg/mL were added. The whole samples were incubated for 2 h with shaking in an incubator chamber at 37 $^{\circ}\text{C}$. The samples were spin down at 4500 rpm for 10 min to obtain the plasma (plasma would be red in color if hemolysis happened). The plasma were collected [(100 μL

plasma + 1 mL Na_2CO_3 (0.01%)]. The OD values were read at 450, 380, and 415 nm. The plasma hemoglobin can be found out according to the following equation

$$\text{plasmaHb} = \{(2A_{415}) - [A_{380} + A_{450}]76.25\}$$

The obtained sample values were compared with that of control (blood + saline). To obtain 100% hemolysis, we lysed cells by dispersion in 1% trypsin. Each concentration was evaluated in triplicate.

Analytical Determinations. FT-IR spectra of materials were carried out using KBr tablets (1% w/w of product in KBr) with a resolution of 4 cm^{-1} and 100 scans per sample on a Perkin-Elmer Spectrum RX1 apparatus. Surface charge and thereby the stability of the same system was obtained by zeta potential measurements (DLS-ZP/Particle Sizer NicompTM 380 ZLS). The particle size was measured by Dynamic light scattering (DLS-ZP/Particle Sizer NicompTM 380 ZLS) taking the average of 3 measurements. The surface morphology of nanogels was analyzed by SEM (JEOLJSM-6490LA) and AFM (JEOL JSPM-5200). The probe sonication was done with a Vibra-Cell sonicator with working power of 130 W, frequency 20 kHz, and voltage of 230 V. Electrochemical measurements were performed in a three-electrode cell configuration with a platinum counter electrode, gold disk working electrode, and an Ag/AgCl/KCl reference electrode. All potentials were determined with respect to the reference electrode and were controlled by potentiostat-galvanostat (Autolab). The surface of the gold plates was polished by 0.05 μm alumina powder followed by treatment with concentrated H_2SO_4 . Then the gold electrodes were thoroughly washed with doubly distilled water. Electrochemical studies were carried out in 5 mM $\text{Fe}(\text{CN})_6^{4-/3-}$. Before measurements gold electrodes were cycled in the electrolyte in the potential region from -1.5 to 1 V. For cyclic voltammetry studies gold disk working electrode was modified with CdTe quantum dots and CdTe-QD-CNGs complex. Pretreated gold electrodes were soaked in MPA capped CdTe QD and CdTe-QD-CNGs solution. Modified Au electrodes were cycled in 5 mM $\text{Fe}(\text{CN})_6^{4-/3-}$ from -1.5 to 1 V at a potential sweep rate of 20 mV s^{-1} .

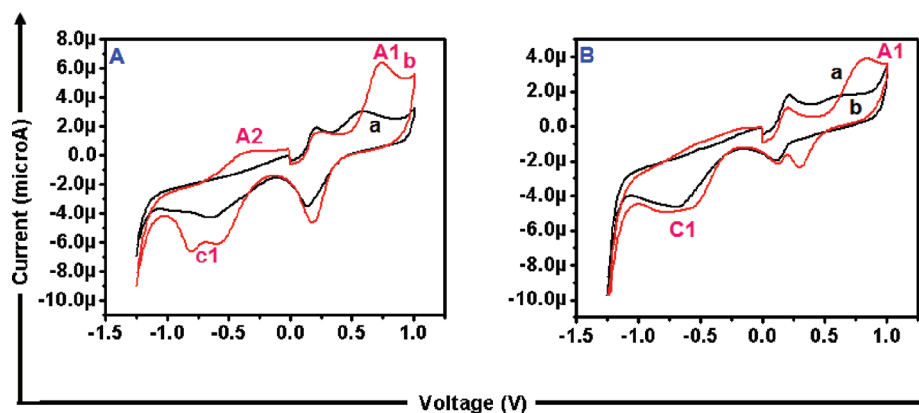


Figure 8. Cyclic voltammograms of (A) (a) bare Au disk electrode (black line) and (b) QD/Au electrode (red line). (B) Cyclic voltammograms of (a) CNGs/Au electrode (red line) and (b) QD-CNGs/Au electrode (black line).

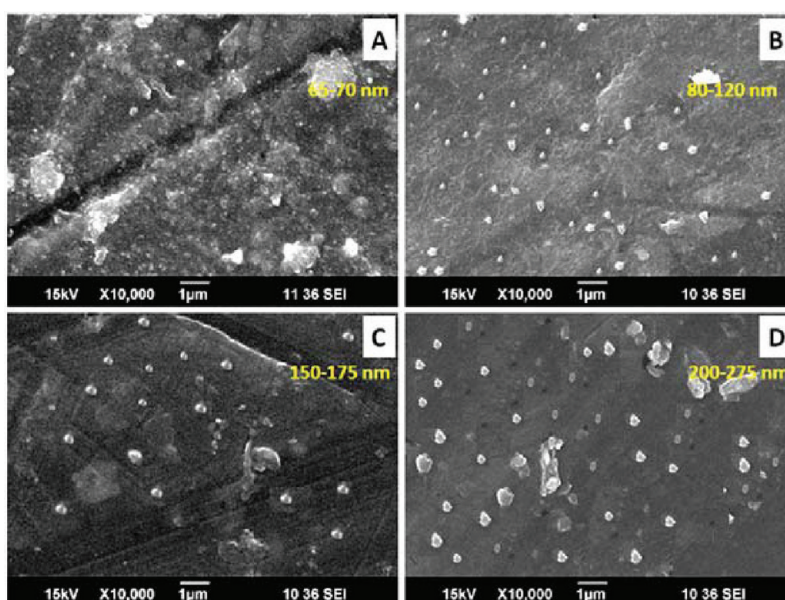


Figure 9. BSA dose-dependent particle size of CNGs with (A) 5; (B) 10; (C) 20, and (D) 40% BSA, respectively.

Statistics. Statistical analysis of the data was performed via one-way analysis of variance (ANOVA) using origin software; a value of $p < 0.05$ was considered significant. ($n = 3$).

RESULTS AND DISCUSSION

CdTe-QDs characterization. Luminescence of the collected QD samples varied from bright green to red as shown in Figure 3. This variation in the luminescence corresponds to the increase in the size of the particle, which is according to literature varies from 2 to 5 nm. The absorption and emission spectra of three different-sized CdTe QDs are shown in Figures 4A and 5. Absorption (Figure 5A) and PL spectra (Figure 5B) shows characteristic peaks of CdTe QDs at their band edges, the shift of first exciton peak ($1S_{3/2} - 1S_e$) to lower wavelength with decreasing particle size represents size quantization effect in these particles (Figure 4B). The XRD analysis was done to find out the crystallographic nature of the CdTe QDs (Figure 4C).

Zeta potential of MPA-capped QDs was determined as -45 mV and the QDs were stable for a long period. The particle size of thiol-capped CdTe QDs synthesized in aqueous solution can be determined from the “sizing curve”: the position of the first absorption peak was determined from the sizing curve³⁸ (Figure 4A.) CdTe in this study is passivated using thiol, MPA (mercapto propionic acid), which allows it to control the kinetics of the nanocrystal synthesis, passivate surface dangling bonds, and provide stability, solubility, and surface functionality to the nanoparticles. The absence of S–H stretching mode around $2550\text{--}2600\text{ cm}^{-1}$ in the FTIR Spectra (see the Supporting Information, Figure S1 for better clarification) of CdTe capped with MPA, indicates that the Thiol group of MPA bound to the surface of QDs through Cd–S bond. The peak at 3483 and 1641 cm^{-1} indicates O–H stretching and the C=O conjugated stretching vibrations that are due to the weakening of C=O because of resonance.^{39–41}

Synthesis of CNGs through Regeneration Chemistry and Multifunctionalization with QDs. To fabricate chitin-CdTe

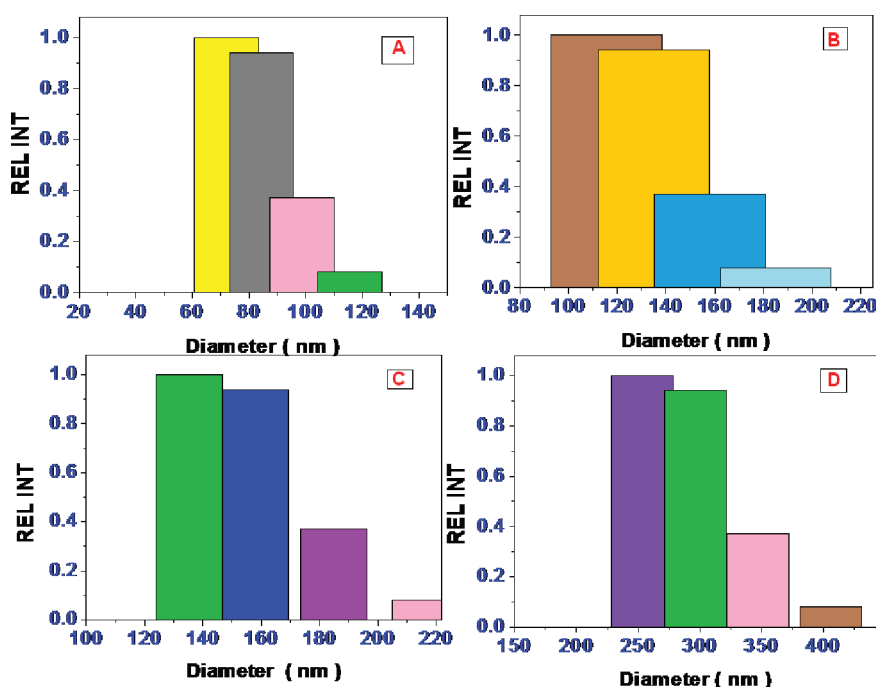


Figure 10. BSA dose-dependent particle size distribution for CNGs in DLS with (A) 5, (B) 10, (C) 20, and (D) with 40% BSA in CNGs.

hybrid nanogels, we adopted a strategy wherein a controlled regeneration of chitin to nanogel was observed. Chitin nanogels in this case plays two roles, one as a pH responsive carrier and the other as a shell coating on CdTe QDs. CdTe-conjugated nanogels are specially designed as an optical identification code for bio sensing and cellular imaging. The reversible pH-induced volume phase transitions of the chitin nanogels will modify the physicochemical environment of the embedded QDs for the conversion of chemical/biochemical signals to optical signals and regulate the release of anticancer drugs and proteins trapped in the gels in the typical abnormal pH range of 5–7.4 found in microenvironments of extracellular tissues of tumors. Briefly, chitin nanogel preparation involves regeneration of chitin and the resulting residues were probe sonicated to get the nanogels of optimum size for the drug delivery applications. Here, the important parameters involved are probing time and amplitude at which the regeneration to nanogels takes place. As the amplitude and time of probing increases, the particle size seems to be decreased (Table 1; refer to the Supporting Information, Table 3).

Our strategy to prepare the multifunctional chitin-CdTe hybrid nanogels involves first, the synthesis of stimuli responsive chitin nanogels, followed by the in situ synthesis of CdTe QDs inside the nanogels. The chitin-CdTe hybrid nanogels were prepared by the physical cross-linking/coating of chitin nanogels on the QDs. chitin chain in solution is in cationic polyelectrolyte form, which tends to ease the formation of specific structures via electrostatic interactions with QDs and form interpolymer complexes. The QDs are terminated with carboxyl functionalities with the intension of reducing the toxicity, where the Cd²⁺ can easily be attached with either –OH and/or –NH₂ groups of CNGs, making more accurate bonding as shown in the Figure 11.

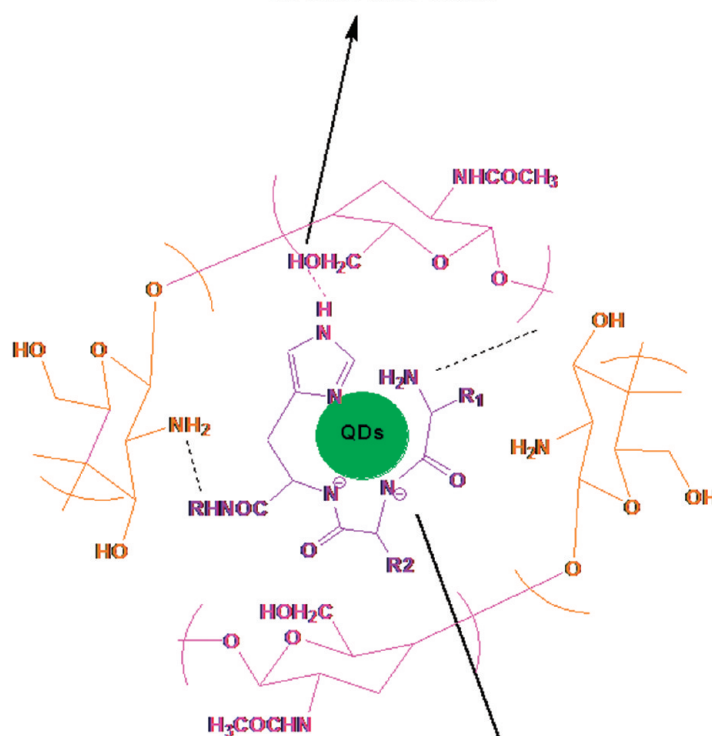
For the nanogels preparation, we adopted a novel regeneration chemical route, where we mixed the chitin solution in an equal volume of the methanol solution until the regeneration of chitin takes place. The resulting mixture was immediately centrifuged to get the pellet, which is then probed at higher amplitude of 75%,

for 5 min to get optimum sized particle as shown in the Supporting Information, Table 3. The process repeated several times until the stable nanosuspension has formed. The interplay of other interactions, such as hydrophobic association of major functionalities may also contribute toward the stability of the nanogels. The nanogels were selected for further immobilization of CdTe QDs. The resulting hybrid nanogels are coded as QD-CNGs. Both –NH₂ and –OH groups of chitin are able to link metal ions in the QDs. The amino groups of chitin are mostly protonated (pH < pK_a) and positively charged, thus will not bind the Cd²⁺ ions. Therefore, most of Cd²⁺ ions are loaded into the nanogels through the coordination between the Cd²⁺ ions and the OH groups of chitin chains.

Size and Morphology of the Nanogels. The nanogels carriers in the size range of 10 to 100 nm have actual advantages to improve the blood circulation time and enhance the extravasation rate into permeable tissues such as tumors. Figure 6A and D shows the DLS spectra of the CNGs and BSA-QD-CNGs; whereas Figure 6B and E is the SEM images for the CNGs and BSA-QD-CNGs with their respective magnified images inset (6b1 and 6e1). SEM and AFM (Figure 6C and c1) analysis confirms that CNGs are nearly spherical in shape with an average diameter of <100 nm. The BSA-QD-CNGs showed an increased particle size in all analysis of DLS, SEM, and AFM (Figure 6D, E, e1, F, and f1), suggesting that a sufficient amount of BSA might be entrapped inside the QD-CNGs.

Zeta Potential Measurements. The size of the CNGs simply controlled by tuning the probing parameters such as time (s); amplitude(%) and energy (Joules) during probing period (Table 1 and the Supporting Information, Table 3). The nanogels presented positive surface charge at pH 7.0. Surface charge and thereby the stability of the prepared nanogels were determined by zeta potential measurements. Zetapotential value for the CNGs was found to be +26.34 mV. This value lies in the stable range, indicating that the nanogels were stable (Figure 2Ba & e) and possess positive surface charge. The whole

Hydrogen bonding between N-terminal of 3rd residue histidine of BSA and CNGs



Square planar co-ordination of Cd²⁺ in MPA-Capped CdTe QDs

Figure 11. Plausible interaction chemistry between the MPA-capped CdTe, BSA, and CNGs.

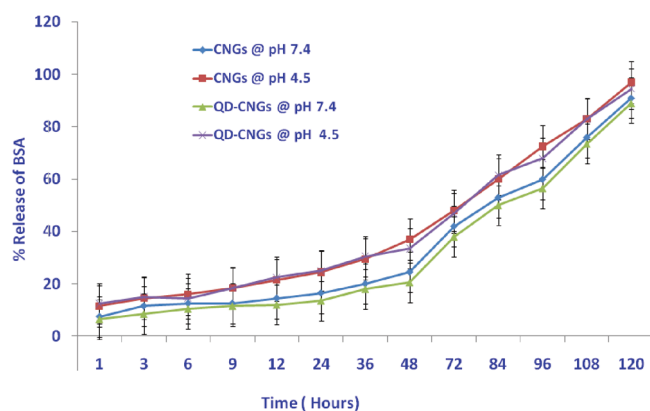


Figure 12. BSA release from the CNGs and QD-CNGs in a controlled manner in PBS (pH 7.4) and (pH 4.5).

experiments were analyzed in water medium after centrifuging the nanogels at 12,000 rpm for 15 min. The QD-CNGs showed +22.34 mV, whereas the BSA-QD-CNGs showed a decrease in zeta potential value as +20.21 mV. The reduction in zeta potential values could be associated with prominent interactions among the major functionalities in QDs and CNGs.

Characterization by FTIR. The FT-IR analysis was performed to analyze the possible interactions between the components (Figure 7) in the CNGs and BSA-QD-CNGs. We analyzed the regenerated materials with the control α -chitin. The material is pure chitin with split transmittance peaks at 1660 and 1638 cm^{-1}

corresponding to the amide I region and transmittance peak at 1560 cm^{-1} corresponding to the amide II region. The spectrum is lacking a signal at 1540 cm^{-1} , where proteins would normally give rise to absorption. From this, it is evident that the chitin is pure of any protein material.⁴¹

As expected, the in situ immobilization of the CdTe QDs into the nanogels almost has no effect on the characteristic absorption peaks of $-\text{COOH}$ groups of and amide bands of chitin (1580–1650 cm^{-1}) in FTIR spectra (Figure 7) because of the successful protection of these functional groups during the loading process of Cd^{2+} ions.

The peaks of pure BSA at 3430, 3062, 1652, and 1531 cm^{-1} are assigned to the stretching vibration of $-\text{OH}$, amide I (mainly $-\text{NH}$ stretching vibration), amide-II (mainly $\text{C}=\text{O}$ stretching vibrations), and amide-III (the coupling of bending vibrates of $\text{N}-\text{H}$ and stretching vibrates of $\text{C}-\text{N}$) bands, respectively (Figure 7C). Here in the encapsulated CNGs, the major amide peaks has been shifted to lower frequency region because of the strong interaction with the BSA molecules, suggesting most of the proteins would be inside the nanogels (Figure 7F). The bond length of the CNGs would be disturbed by the Ca^{2+} ions which would have resulted in the lower frequency shifting of the wavenumber in nanoformulations. Ca^{2+} ions are good cross-linking agents for the negatively charged species like $-\text{NHCOCH}_3$, $-\text{COOH}$ etc. Since chitin has a lot of such groups, it is possible for the Ca^{2+} to well cross-link with them, thus perturbing the ordinary bonding of $-\text{NHCOCH}_3$ in the nanoscale regime.³⁹ Because of the complex interaction nature of QDs with BSA and CNGs, there were no characteristic peaks observed in the case of BAS-QD-CNGs as

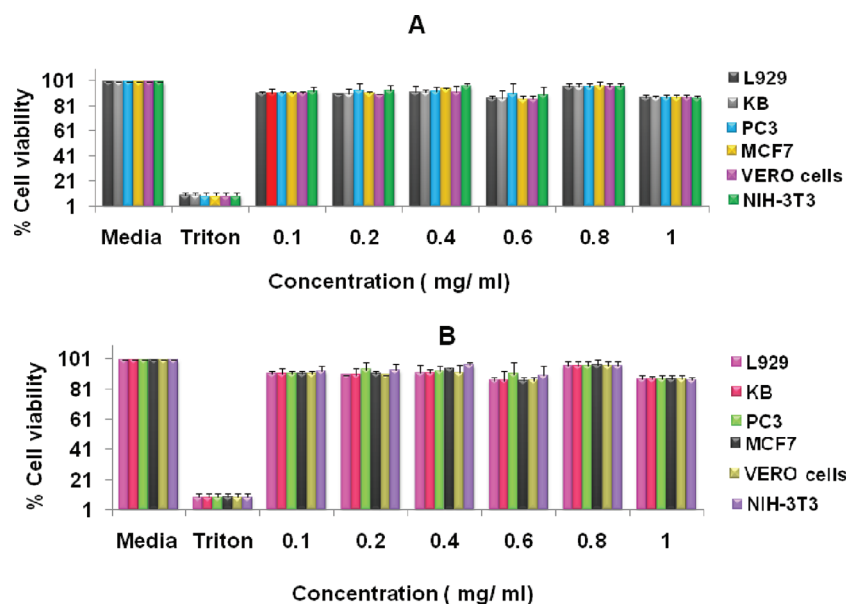


Figure 13. Cytotoxicity studies on (A) CNGs and (B) BSA-QD-CNGs after 24 h exposure on different cell lines.

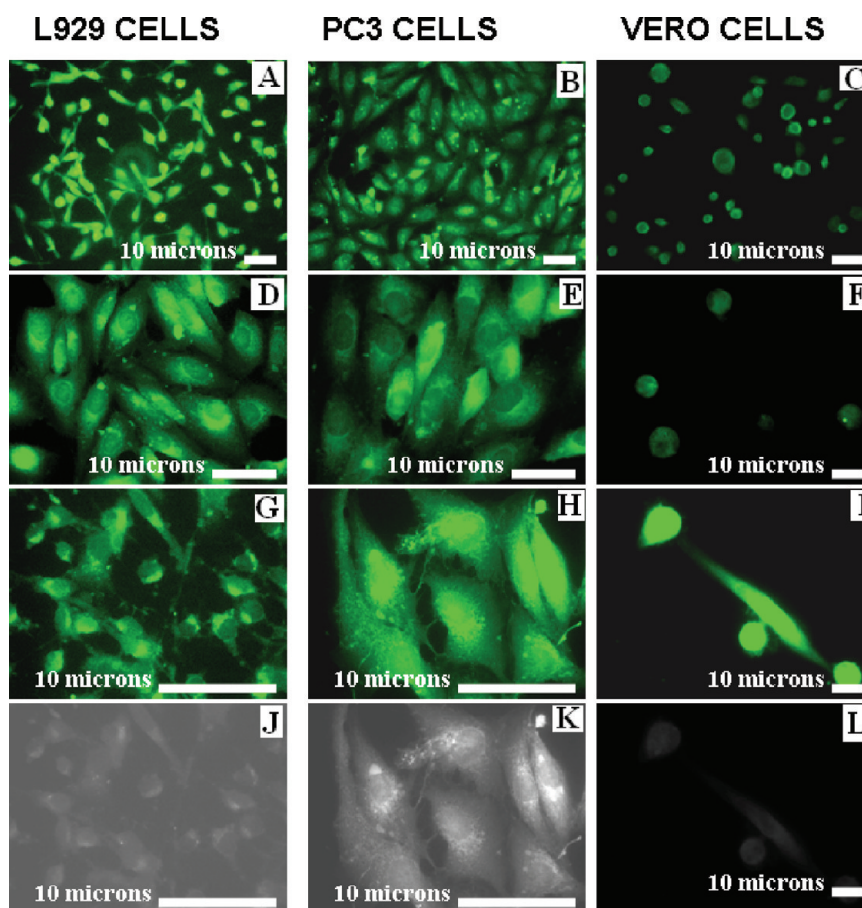


Figure 14. Cell uptake studies of QD-CNGs after 2 h exposure on L929, PC3, and VERO different cell lines at (A–C) 20 \times , (D–G) 40 \times , and (H, I) 100 \times magnifications. (J–L) represent the bright-field images.

shown in Figure 7F, but there is a sharp peak at 1638 cm^{-1} , which could be due to the carbonyl stretching modes of vibration during the

square planar interaction of Cd^{2+} with the BSA in the BSA-QD-CNGs⁴¹ (refer to Figure 11).

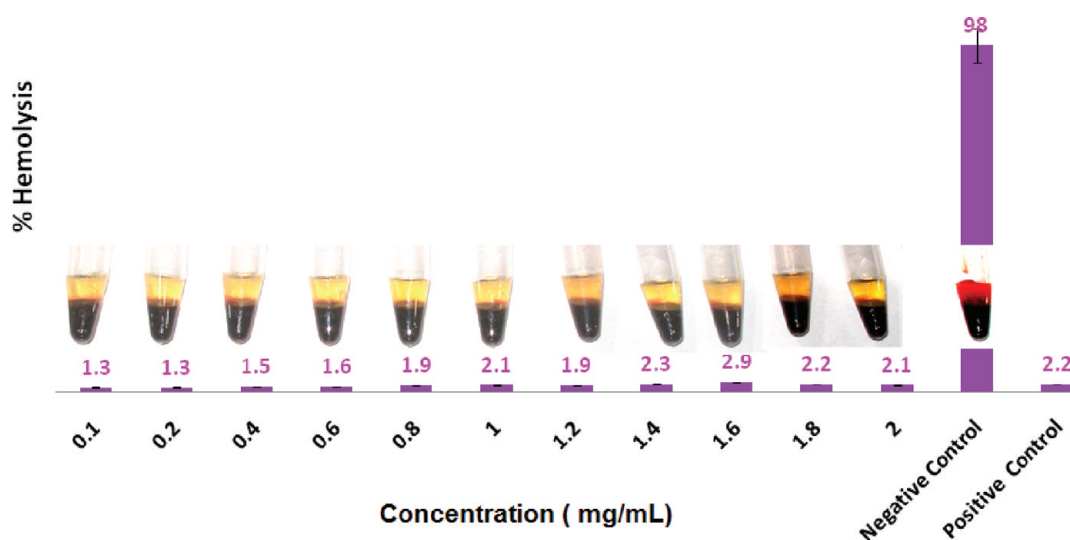


Figure 15. Hemolysis assay of the QD-CNGs at different concentrations after incubation for 2 h.

Electrochemical Analysis of the Nanogels. Figure 8Aa (black line) shows the CV of Au electrode in blank electrolyte, Figure 8Ab shows the CV of CdTe adsorbed Au electrode. When the potential is swept from the open circuit potential (E_{oc}) in the positive direction, an anodic peak A1 at potential regions (0.6–0.8 V), A2 at (–0.3 to 0.5) and a cathodic peak C2 from region (–0.5 to –0.9 V) is observed and corresponds to the oxidation and reduction potentials of MPA capped CdTe QD. Figure 8Ba (red line) shows the CV of CNGs/Au electrode and b (black line) shows the QD-CNGs/Au electrode CV curve, the anodic peak A2 of bare QD on Au electrode disappears when QD is complexed with CNGs, but the oxidation A1 and reduction peaks C1 of CdTe QD do not undergo much shift after complexing it with CNGs, which proves that complexing QD with CNGs does not reduce the electrochemical stability and luminescent properties of the QDs (Figure 2Bc). This is an important observation and is required for the biosensor, as it has to image the cells in the *in vivo* experiments.

BSA Loading Efficiency of the Nanogels. The loading efficiency was the same with different BSA concentrations. Interestingly, the size was increased from 65 to 275 nm with respect to the loading % of the BSA in CNGs. This has been confirmed by SEM and DLS analysis as shown in Figures 9 and 10, respectively. The SEM analysis clearly showing that particle size can be changed with respect to the BSA concentration. The relationship between loading efficiency and the particle size has been tabulated in the Table 2 (see the Supporting Information, Table 2).

The QD-CNGs have also analyzed for the Loading efficiency with BSA, which showed a good loading efficiency of ~90% with 10% BSA. The plausible interaction chemistry of BSA with the QD-CNGs have showed in the Figure 11. There could be a strong hydrogen bonding interaction between the QDs and the N-terminal of third residue histidine of BSA.⁴² The possibility of square planar co-ordination between Cd^{2+} and the BSA has been shown in the Figure 11.

Protein Release Studies from CNGs and QD-CNGs. The BSA was taken as the model protein drug in this study. The release profile was shown in the Figure 12. It is evident from the Figure 12 that the protein is being released from the carrier molecules in a controlled manner. 22% of the BSA was released

within 24 h followed by slow release of 32% even after 72 h, whereas there is a significant increase in the BSA release for both CNGs and QD-CNGs at the acidic pH as shown in the Figure 12. This probably could be due to the acidic degradation nature of CNGs⁴³ as we explained in the Supporting Information, Figure S2. The whole BSA was released within 5 days, suggesting controlled and sustained release is possible by encapsulating BSA on the nanogels. The mechanism of drug release could be pH responsible biodegradation followed by swelling of the CNGs, so that the entrapped BSA can easily be released from the nanogels. The studies indicate that these nanogels could be suitable biodegradable vehicles for growth factors, genes, and hormones in drug delivery and tissue engineering filed.

Cytotoxicity Studies. The nanogels are cytocompatible in all of the concentrations we studied (Figure 13A); similarly, we compared the level of toxicity of BSA-QD-CNGs with the negative control, which are the cells grown in its respective media. It is evident from the Figure 13A that compared to the negative control, almost 90% of cells are viable in all six concentrations of CNGs. These results indicated that the prepared nanogels carriers are nontoxic to L929, KB, PC3, MCF7, VERO, and NIH-3T3 cells. The same experiments we analyzed with BSA-QD-CNGs in the same concentration range (0.1–1 mg/mL) (Figure 13B). From our experimental observations it is evident that the BSA-QD-CNGs in the same concentration did not show any toxicity on to any of the cell lines.

Fluorescent Microscopy for Cell Imaging Using QD-CNGs. It is good observation that the fluorescence of the QD-CNGs would not completely quench even after cellular localization, thus the QD-CNGs can be applied for cell-labeling under physiologically important pH conditions. Figure 14 shows the luminescence images of the L929, VERO, and PC3 cells after being stained with QD-CNGs for 2 h. There were no changes in cellular morphology even after incubation for 24 h with the QD-CNGs (see the Supporting Information, Figure S3), correlating these data with the MTT assay for 24 h. It is clear that the cells can readily phagocytose the small sized QD-CNGs. The bright spots are attributed to the CdTe QDs encapsulated inside the CNGs, which can illuminate the entire cell. These bright spots are mainly distributed in the cytoplasm and perinuclear region of the cells. It is thus obvious that these

probes do not give dark regions in the cell, and simply areas where the nanogel did not permeate are clear, rendering the QD-CNGs suitable for cell-labeling markers. Although nowadays semiconductor QDs have been widely applied for cellular imaging, such a chitin nanogel system designed for the optical probe would potentially facilitate a simultaneous combination of optical diagnosis, distribution of nanopolymeric drug conjugates, and monitoring on the response to drug treatments. Most of the QD related work has been showing the retention of the QDs inside the cell for a few hours, wherein here we could demonstrate their retention for a higher time span of 24 h, showing there is no toxicity to the cells⁴⁴ (refer to the Supporting Information, Figure S3).

Blood Compatibility Studies of the Nanogels. The hemocompatibility of biomaterials is an important parameter as these materials might be exposed in blood and damaged the erythrocytes in certain degree to form the thrombus. Hemolysis assay was carried out to evaluate the blood compatibility of QD-CNGs. The results in Figure 15 showed that the hemolytic ratio of the sample was far below 5%, the critical safe hemolytic ratio for biomaterials according to ISO/TR 7406, which indicated that all samples from QD-CNGs are hemocompatible.

CONCLUDING REMARKS

Chitin nanogels have been prepared as first time in literature to the best of our knowledge for a variety of biomedical applications. The multifunctional chitin hybrid nanogels can be prepared in an aqueous solution via in situ immobilization of MPA-capped CdTe QDs into the chitin nanogels, which can easily be loaded with BSA protein drug (BSA-QD-CNGs). The distinction in the stability of hybrid nanogels is important for the designed multiple functions. The results reported here suggest that nanogels with excellent stability and reversible physical property change in response to a pH change can successfully integrate the optical pH-sensing and cellular imaging ability, regulated protein delivery, and excellent cytocompatibility into a single nano-object. The QDs conjugated nanogels could enter and illumine the cells, detect the change in pH, provide a pH-regulated release of proteins like BSA in the typical abnormal pH range of 5–7.4 found in pathological zone, which provides potential for monitoring on the response to drug treatments and improving the therapeutic efficiency. These results could be useful for throwing light on the fact that, simultaneous drug delivery along with imaging and biosensing for future nanomedicines derived from chitin.

ASSOCIATED CONTENT

Supporting Information. Biodegradation of chitin (control); chitin nanogels (CNGs) with and without lysozyme; swelling studies for the same; individual FTIR spectra of MPA-Capped CdTe QDs; 24 h exposed QD-CNGs on L929 and PC3 cells; the weight concentrations of BSA and QDs in hybrid BSA-QD-CNGs; relation between loading efficiency and particle size of the BSA-loaded-CNGs and relationship between probing parameters (such as power, time, energy) with the particle size. This material is available free of charge via the Internet at <http://pubs.acs.org/>.

AUTHOR INFORMATION

Corresponding Author

*E-mail: rjayakumar@aims.amrita.edu or jayakumar77@yahoo.com. Tel.: +91 484 2801234. Fax: +91 484 2802020.

ACKNOWLEDGMENT

The Department of Biotechnology, Government of India supported this work, under a center grant of the Nanoscience and Nanotechnology Initiative program (ref. no. BT/PR10850/NNT/28/127/2008). N.S.R. acknowledges the Council of Scientific and Industrial Research (CSIR) for the financial support through Senior Research Fellowship (SRF) {Award 9/963 (0017)2K11-EMR}. This work is also partly supported by Nanomission, Department of Science and Technology, Government of India. The authors are thankful to Lekha P. Mohandas and Mr. Sajin P. Ravi for their technical support during cyclic voltametry, QD synthesis, and SEM analysis. Special thanks to our colleagues at amrita centre for nanosciences and molecular medicine, AIMS Kochi, for their support throughout this work.

REFERENCES

- (1) Jayakumar, R.; Deepthy, M.; Manzoor, K.; Nair, S. V.; Tamura, H. *Carbohydr. Polym.* **2010**, *82*, 227–232.
- (2) Lim, I. I. S.; Njoki, P. N.; Park, H. Y.; Wang, L.; Mott, D. I. *Nanotechnology* **2008**, *19*, 305102.
- (3) Michalet, X.; Pinaud, F. F.; Bentolila, L. A.; Tsay, J. M.; Doose, S.; Li, J. J. *Science* **2005**, *307*, 538–544.
- (4) Cui, B.; Wu, C.; Chen, L.; Ramirez, A.; Mobley, W. C.; Chu, S. *Proc. Natl. Acad. Sci. U.S.A.* **2007**, *104*, 23666–71.
- (5) Park, K.; Lee, S.; Kang, E.; Kim, K.; Choi, K.; Kwon, I. C. *Adv. Funct. Mater.* **2009**, *19*, 1553–1566.
- (6) Zaman, M. B.; Baral, T.; Zhang, J. B.; Whitefield, D.; Yu, K. S. *J. Phys. Chem. C* **2009**, *113*, 496–499.
- (7) Kim, S.; Lim, Y. T.; Soltesz, E. G.; De, Grand, A. M.; Lee, J.; Nakayama, A. *Nat. Biotechnol.* **2004**, *22*, 93–97.
- (8) Tan, W. B.; Jiang, S.; Zhang, Y. *Biomaterials* **2007**, *28*, 1565–1571.
- (9) Bhang, S. H.; Won, N.; Lee, T.; Jin, H.; Nam, J.; Park, J. *ACS Nano* **2009**, *3*, 1389–1398.
- (10) Lee, H. A.; Imran, M.; Monterio-Riviere, N. A.; Colvin, V. L.; Yu, W. W.; Rvler, J. E. *Nano Lett.* **2007**, *7*, 2865–2870.
- (11) Boussif, O.; Lezoualch, F.; Zanta, M. A.; Mergny, M. D.; Scherman, D.; Demeneix, B. *Proc. Natl. Acad. Sci. U.S.A.* **1995**, *92*, 7297–7301.
- (12) Young, S. H.; Rozengurt, E. *Am. J. Physiol. Cell. Phys.* **2006**, *290*, 728–732.
- (13) Zhang, J.; Xu, S.; Kumacheva, E. *J. Am. Chem. Soc.* **2004**, *126*, 7908–7914.
- (14) Jung, K. O.; Daniel, J. S.; Krzysztow, M. *Biomacromolecules* **2007**, *8*, 3326–3331.
- (15) Stuart, M. A. C.; Huck, W. T. S.; Genzer, J.; Müller, M.; Ober, C.; Stamm, M. *Nat. Mater.* **2001**, *9*, 101–113.
- (16) Wu, W.; Zhou, T.; Zhou, S. *Chem. Mater.* **2009**, *21*, 2851–2861.
- (17) Gong, Y.; Gao, M.; Wang, D.; Mohwald, H. *Chem. Mater.* **2005**, *17*, 2648–2653.
- (18) Fernando, R. D. A.; Sergio, P. C. *Carbohydr. Polym.* **2004**, *75*, 214–221.
- (19) Peter, M.; Sudheesh Kumar, P. T.; Binulal, N. S.; Nair, S. V.; Tamura, H.; Jayakumar, R. *Carbohydr. Polym.* **2009**, *78*, 926–931.
- (20) Kashappa, G. H. D.; Hyun, J. P. *Drug Dev. Res.* **2005**, *64*, 114–128.
- (21) Thanou, M.; Verhoef, J. C.; Junginger, H. E. *Adv. Drug Delivery Rev.* **2001**, *52*, 117–126.
- (22) Muzzarelli, R. A. A. *Carbohydr. Polym.* **1988**, *8*, 1–21.
- (23) Gerrit, B. *Adv. Drug Delivery Rev.* **2001**, *2*, 145–150.
- (24) Jayakumar, R.; Chennazhi, K. P.; Muzzarelli, R. A. A.; Tamura, H.; Nair, S. V.; Selvamurugan, N. *Carbohydr. Polym.* **2010**, *79*, 1–8.
- (25) Jayakumar, R.; Prabakaran, M.; Nair, S. V.; Tokura, S.; Tamura, H.; Selvamurugan, N. *Prog. Mater. Sci.* **2010**, *55*, 675–709.

- (26) Richardson, S. C. W.; Kolbe, H.V. J.; Duncan, R. *Int. J. Pharm.* **1999**, *178*, 231–243.
- (27) Huang, M.; Khor, E.; Lim, L. Y. *Pharm. Res.* **2004**, *21*, 344–353.
- (28) Vander, L.I. M.V.; Kersten, G.; Fretz, M. M.; Beuvery, C.; Verhoef, J. C.; Junginger, H. E. *Vaccine* **2003**, *21*, 1400–1408.
- (29) Xu, Y.; Du, Y. *Int. J. Pharm.* **2003**, *250*, 215–226.
- (30) Calvo, P.; Remunan-Lopez, C.; Vila-Jato, C. L.; Alonso, M. J. *J. Appl. Polym. Sci.* **1997**, *63*, 125–132.
- (31) Bhattarai, N.; Gunn, J.; Zhang, M. *Adv. Drug Delivery Rev.* **2010**, *62*, 83–99.
- (32) Mao, S.; Sun, W.; Kissel, T. *Adv. Drug Delivery Rev.* **2010**, *62*, 12–27.
- (33) Wu, W.; Aiello, M.; Zhou, T.; Berliner, A.; Banerjee, P.; Zhou, S. *Biomaterials* **2010**, *31*, 3023–3031.
- (34) Tannock, I. F.; Rotin, D. *Cancer Res.* **1989**, *49*, 4373–4384.
- (35) Stubbs, M.; Mc Sheehy, P. M. J.; Griffiths, J. R.; Bashford, C. L. *Mol. Med. Today.* **2000**, *6*, 15–19.
- (36) Coakley, R. D.; Grubb, B. R.; Paradiso, A; M.; Gatzky, J. T.; Johnson, L. G.; Kreda, S. M. *Proc Natl. Acad. Sci. U.S.A.* **2003**, *100*, 16083–16088.
- (37) Tamura, H.; Nagahama, H.; Tokura, S. *Cellulose* **2006**, *13*, 357–364.
- (38) Rogach, A. L.; Franzl, T.; Klar, T. A.; Flelmann, J.; Gaponik, N.; Lesnyak, V.; Shavel, A.; Eychmüller, A.; Rakovich, Y. P.; Donegan, J. F. *J. Phys. Chem.* **2007**, *111*, 14637.
- (39) Sanoj Rejinold, N.; Muthunayanan, M.; Deepa, N.; Chennazhi, K. P.; Nair, S. V.; Jayakumar, R. *Int. J. Biol. Macromol.* **2010**, *47*, 37–43.
- (40) Sanoj Rejinold, N.; Muthunayanan, N.; Chennazhi, K. P.; Nair, S. V.; Jayakumar, R. *J. Biomed. Nanotechnol.* **2011**, *161*, 461–472.
- (41) Mi-Kyeong, J.; Byeong-Gi, K.; Young-Il, J.; Chang, H. L.; Jae-Woon, N. *J. Polym. Sci., Part A: Polym. Chem.* **2004**, *42*, 423–432.
- (42) Zhang, Y.; Akhilesh, S. *Inorg. Chem.* **2000**, *12*, 3057–3064.
- (43) Raemdonck, K.; Joseph, D.; De Smedt, S. *Soft Matter* **2009**, *5*, 707–715.
- (44) Martin, J. D.; Clift; Christina, B.; Barbara, R. R.; David, M. B.; Stone, V. *Toxicol.* **2011**, *286*, 58–68.